Supplementary Material for:

"Beyond surface fluxes: Observational and computational needs of multilayer canopy models – a walnut orchard test case"

Gordon B. Bonan[a], **Sean P. Burns**[a,b], **and Edward G. Patton**[a]
[a]*NSF National Center for Atmospheric Research, Boulder, Colorado, USA*
[b]*Department of Geography, University of Colorado, Boulder, USA*

1. **Supplemental Tables S.1 to S.4**
2. **Supplemental Figures S.1 to S.19**

Table S.1
The nominal heights of the temperature-humidity (T/RH), sonic anemometer (CSAT3), and krypton hygrometer sensors on the 30-m vertical tower during CHATS. For each nominal height, the true sensor height above the ground level and serial number are provided, The krypton hygrometer is assumed to be at the same height as the CSAT3. The CSAT3 booms were nominally pointed toward the west while the T/RH booms were pointed toward the east. For the CSAT3, the boom angle and the planar fit coefficients (lean angle, lean azimuth angle, and vertical wind w offset) are provided at each level. For additional details see Horst (2019).

	Actual Heights [m]			CSAT3 Additional Details			
Nominal Height [m]	T/RH	CSAT3	Krypton	Boom Angle[a] [deg]	Lean [deg]	Lean Azimuth [deg]	w offset
29	28.51 (sn 104)	29.03 (sn 0744)		275.4	1.5	61.0	0.02
23	22.55 (sn 701)	23.07 (sn 1117)	23.07 (sn 1525)	275.4	1.3	57.7	0.00
18	17.52 (sn 005)	18.04 (sn 0738)		275.4	1.6	47.1	0.00
14	13.57 (sn 101)	14.52[b] (sn 1123)	14.52[c] (sn 1393) (sn 1397)	275.4	1.3	19.0	−0.01
12.5		12.54 (sn 0743)		275.4	1.2	75.8	−0.03
11	11.12 (sn 006)	11.13 (sn 0364)		275.4	1.4	27.1	−0.02
10	10.04 (sn 008)	10.03 (sn 0671)	10.03 (sn 1101)	275.4	2.0	21.8	−0.06
9	9.04 (sn 001)	9.02 (sn 0536)		**274.8**	1.0	12.8	−0.04
7.5	7.65 (sn 502)	7.62 (sn 0540)	7.62 (sn 1394)	275.4	2.4	6.7	−0.02
6	6.07 (sn 204)	6.07 (sn 0740)		275.4	3.0	25.6	−0.03
4.5	4.54 (sn 007)	4.54 (sn 1120)	4.54 (sn 1390)	**275.6**	2.6	27.7	−0.02
3	3.11 (sn 004)	3.11 (sn 0674)		**276.2**	2.2	47.5	0.00
1.5	1.55 (sn 703)	1.54 (sn 0673)	1.54 (sn 1395)	**274.8**	0.9	37.2	0.00

[a] The angle of the CSAT3 boom (degrees from true north) is listed. The 1.5 m, 3 m, 4.5 m, and 9 m boom angles were measured with a datascope/theodolite and are in bold. The boom angle for other levels are estimated/approximated.
[b] On 25 March 2007 (at around 17:00 PST), the 14-m CSAT3 was moved from 14.09 m to 14.52 m to allow raising of the boom to service one of the hot film anemometers.

[c] On 21 May 2007 (at around 14:20 PST), the 14-m krypton hygrometer sn 1393 was replaced with sn 1397.

Table S.2
The May 2007 mean values used as input to the Kljun et al. (2015) footprint model to create the footprints shown in Figs. S.1 and S.2. These mean statistics are based on stability classes (SU, strongly unstable; WU, weakly unstable; NN, near-neutral; WS, weakly stable; SS, strongly stable). Footprint analyses are separated into periods with wind direction (WD) from the north ($270° < \mathrm{WD} < 90°$) and south ($90° < \mathrm{WD} < 270°$). The variables shown are as follows: the number of 30-min samples in each category (N), bulk Richardson number (Ri_b), wind direction (WD), horizontal wind speed (U), Obukhov length (L), friction velocity (u_*), the standard deviation of the crosswind velocity fluctuations (σ_v), and boundary layer depth (z_i). These are the mean values from N samples. Tower-based variables are from the 23-m level. σ_v is approximated as twice u_*, and z_i is estimated.

Stability Class	N	Ri_b [–]	WD [deg from N]	U [m s^{-1}]	L [m]	u_* [m s^{-1}]	σ_v [m s^{-1}]	z_i [m]
Winds from the North								
SU	113	-2.09	318.8	1.4	-27.1	0.30	0.60	400
WU	60	-0.04	358.3	4.1	-97.5	0.55	1.10	600
NN	137	-0.002	347.0	9.3	-115.8	0.91	1.82	800
WS	100	0.07	327.5	3.9	55.1	0.25	0.50	600
SS	34	6.82	329.0	1.5	7.2	0.09	0.19	200
Winds from the South								
SU	111	-1.50	183.7	1.6	-55.0	0.30	0.59	400
WU	131	-0.04	188.4	3.9	-333.1	0.54	1.08	600
NN	139	0.002	196.2	4.5	437.6	0.51	1.01	800
WS	310	0.05	193.0	3.5	60.8	0.24	0.47	600
SS	50	5.26	202.2	1.9	7.9	0.09	0.18	200

Table S.3
Statistics for the number of times that the aerodynamic conductance attains its lower limit (equivalent to a resistance of 500 s m^{-1}) throughout the month of May. Data are for the model only and have not been filtered for wind direction. Data are given for height classes of 0–1 m, 1–2 m, 2–4 m, and $>$ 4 m and by hour of day in six 4-hour time periods. N is the total possible number of data points in each time-height bin. There are 1488 time samples in each 4-hour period (48 5-min timesteps x 31 days), and the number of levels in each height class is 2, 2, 4, and 38, respectively.

	Height Class			
Hour of Day [PST]	0–1 [m] ($N = 2976$)	1–2 [m] ($N = 2976$)	2–4 [m] ($N = 5952$)	$>$ 4 [m] ($N = 56544$)
00:00–04:00	704	311	57	0
04:00–08:00	622	362	206	0
08:00–12:00	0	0	0	0
12:00–16:00	0	0	0	0
16:00–20:00	237	74	27	0
20:00–24:00	74	11	0	0

Table S.4
Statistics for the number of times that the wind speed (U_i) is $\leq$ 0.04 m s^{-1} throughout the month of May. This is the wind speed at which the lower limit to leaf boundary layer conductance (0.2 mol m^{-2} s^{-1}; equivalent to a resistance of 211 s m^{-1}) is attained. Data are for the model only and have not been filtered for wind direction. Data are given for height classes of 0–2 m, 2–4 m, 4–6 m, 6–8 m, and 8–10 m and by hour of day in six 4-hour time periods. N is the total possible number of data points in each time-height bin. There 1488 time samples in each 4-hour period (48 5-min timesteps x 31 days), and the number of levels in each height class is 4.

	Height Class				
Hour of Day [PST]	0–2 [m] ($N = 5952$)	2–4 [m] ($N = 5952$)	4–6 [m] ($N = 5952$)	6–8 [m] ($N = 5952$)	8–10 [m] ($N = 5952$)
00:00–04:00	2132	1781	1135	90	0
04:00–08:00	2042	1579	1062	249	0
08:00–12:00	703	59	0	0	0
12:00–16:00	60	7	0	0	0
16:00–20:00	1242	936	394	37	0
20:00–24:00	476	381	117	0	0

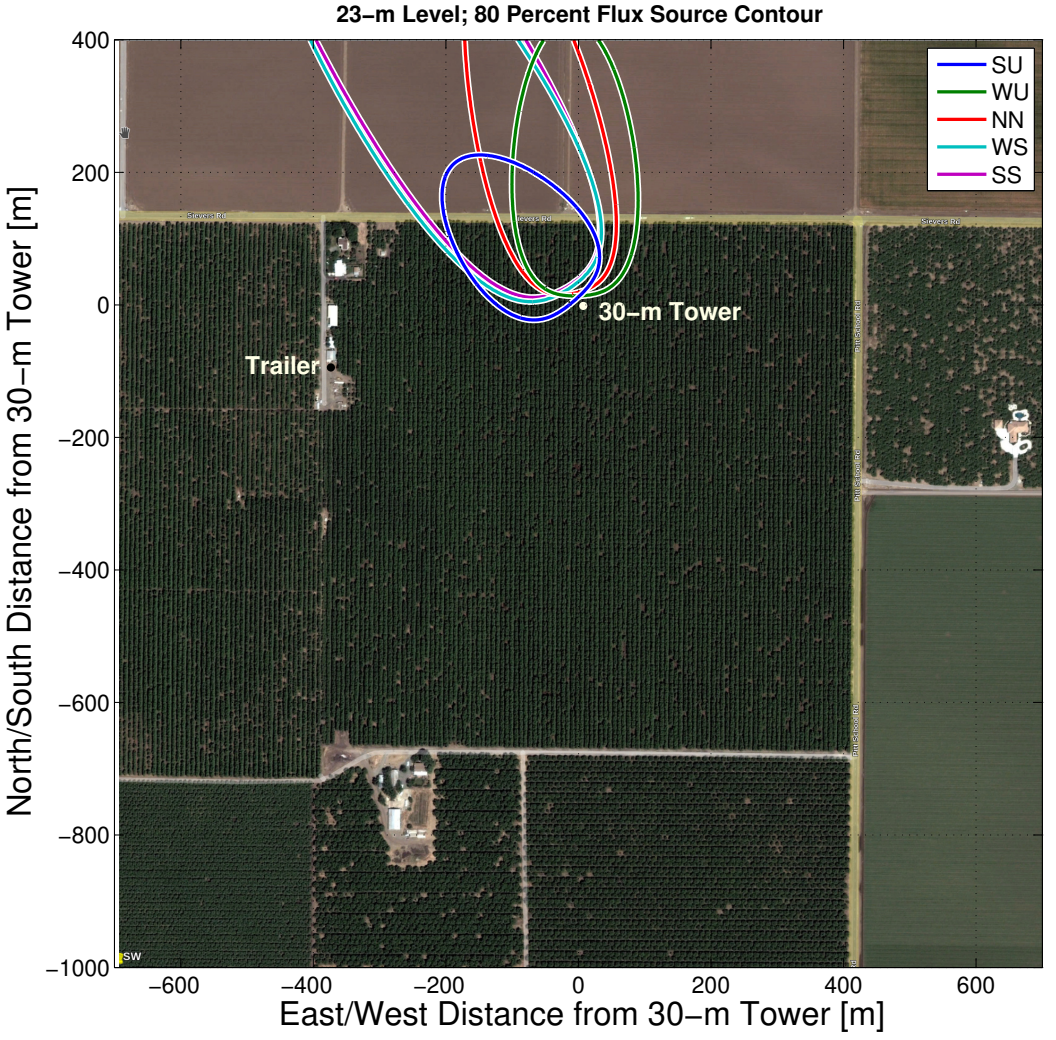

Figure S.1: A Google Earth image (©2025 Maxar Technologies; imagery date 5/23/2010) of the CHATS walnut orchard showing the location of the 30-m tower. Contours of the 80% flux footprint are shown for winds from the north for different stability classes (SU, strongly unstable; WU, weakly unstable; NN, near-neutral; WS, weakly stable; SS, strongly stable). Footprints are calculated based on Kljun et al. (2015). Statistics used to calculate the contours are in Table S.2.

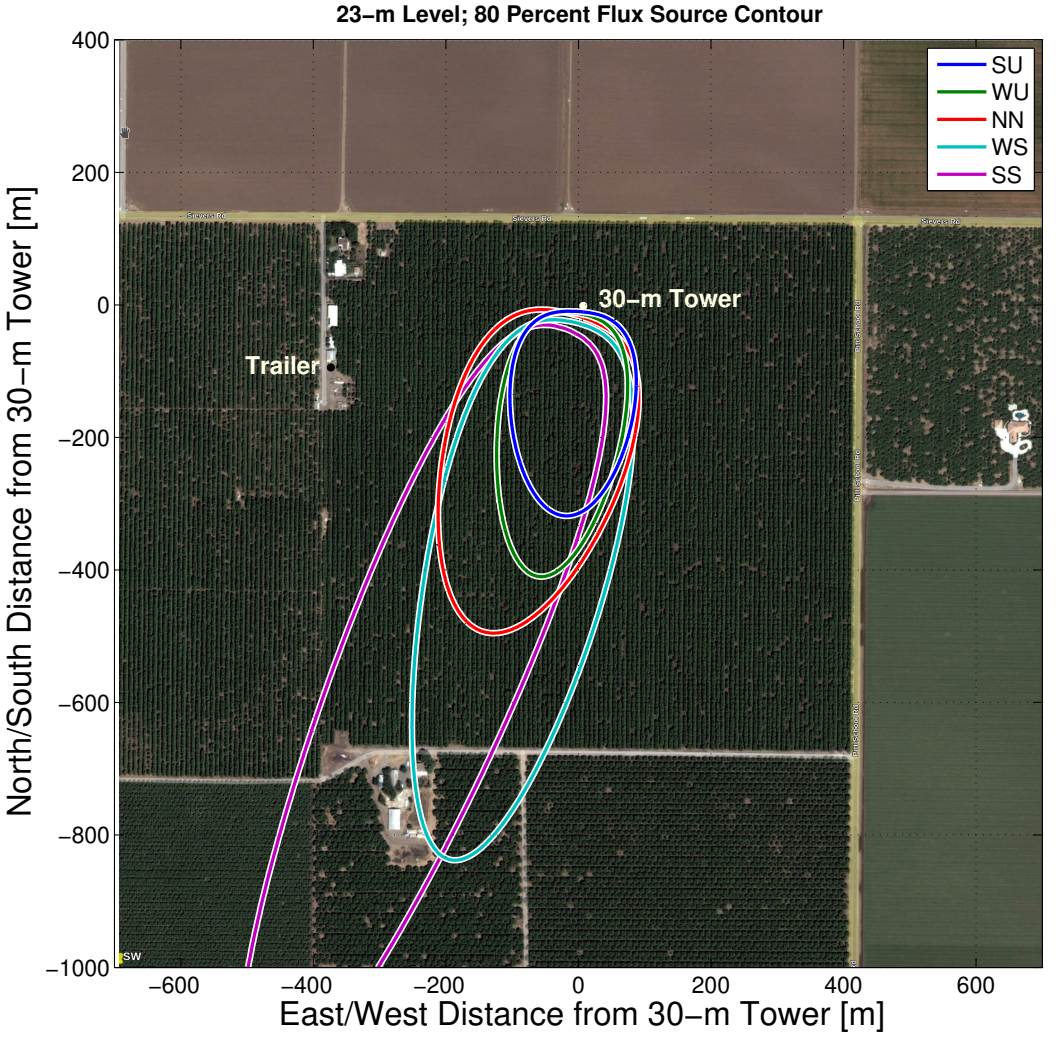

Figure S.2: As in Fig. S.1, but for winds from the south.

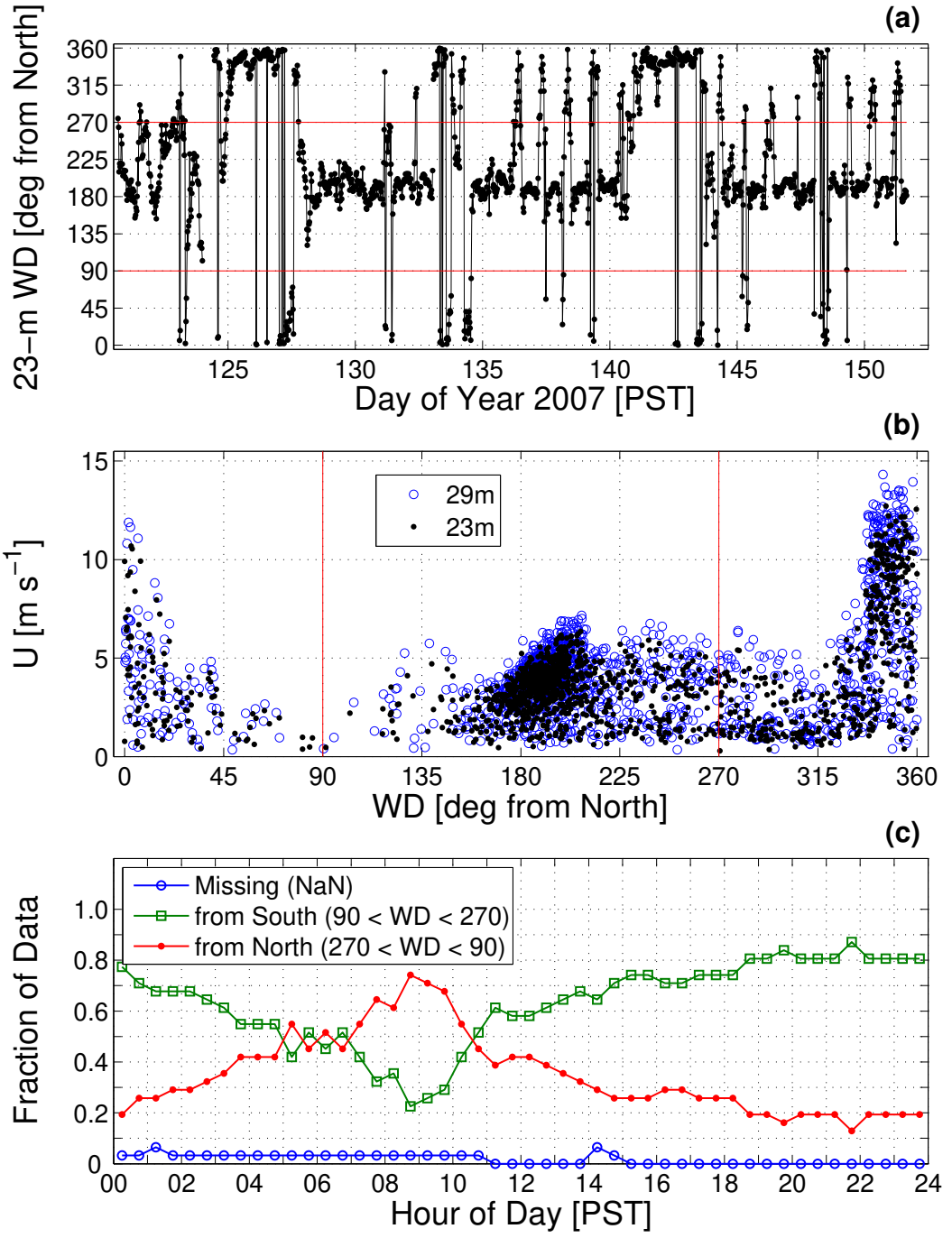

Figure S.3: (a) Time series of 30-min mean observed above-canopy wind direction (WD) for May 2007. **(b)** 30-min mean horizontal wind speed (U) versus WD for two of the above-canopy tower levels. In **(a)** and **(b)**, the red lines indicate the cut-off values used to eliminate the winds coming from the north. **(c)** The diel cycle of 23-m wind direction showing the fraction of 30-min samples that are missing due to instrument problems, coming from the north, and coming from the south.

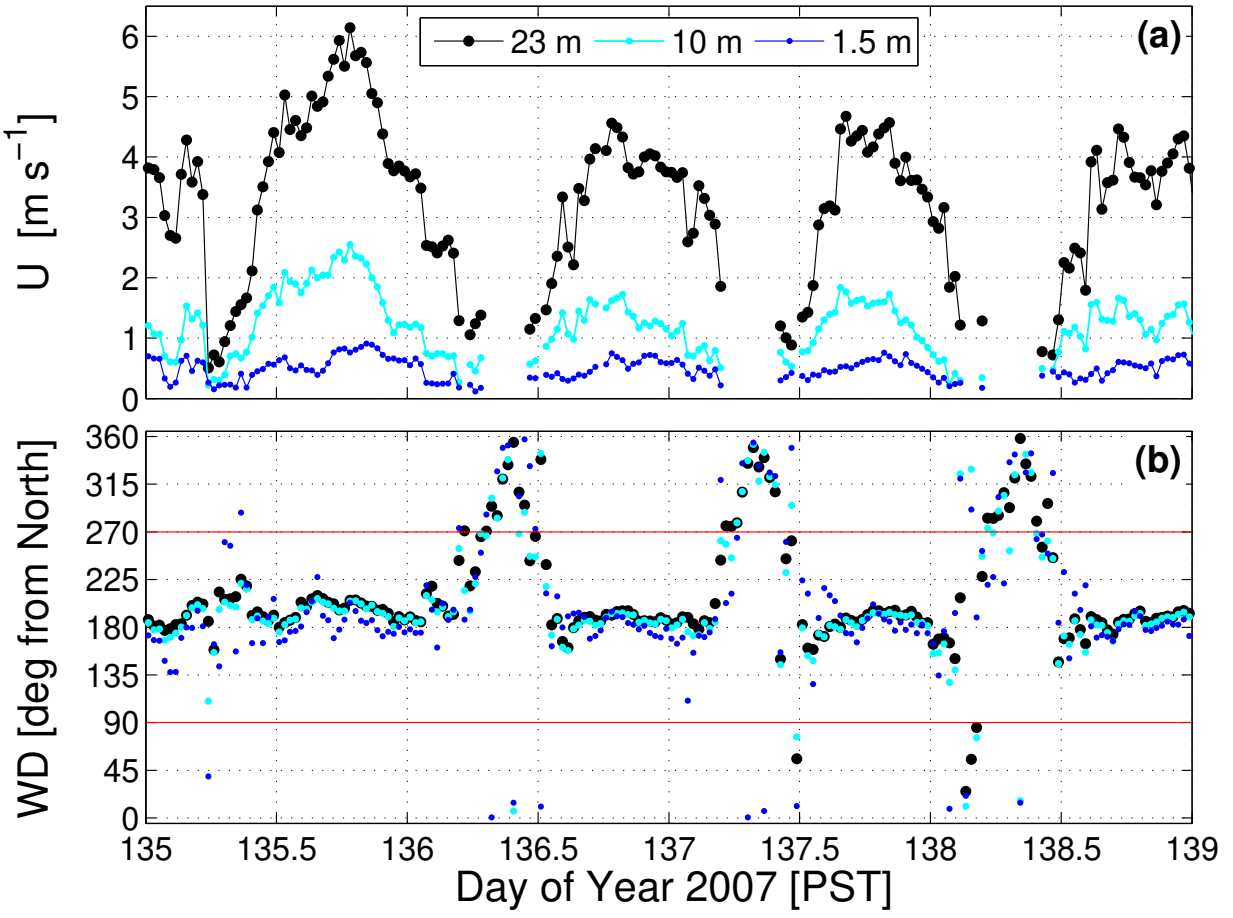

Figure S.4: Time series of 30-min mean **(a)** observed horizontal wind speed (U) for above-canopy, canopy-top, and subcanopy levels, and **(b)** observed wind direction (WD) from the same levels. The legend above **(a)** applies to both panels. In **(a)**, U data have been removed when WD is from the north (i.e., 0–90°, 270–360°), as shown by the red lines in panel **(b)**.

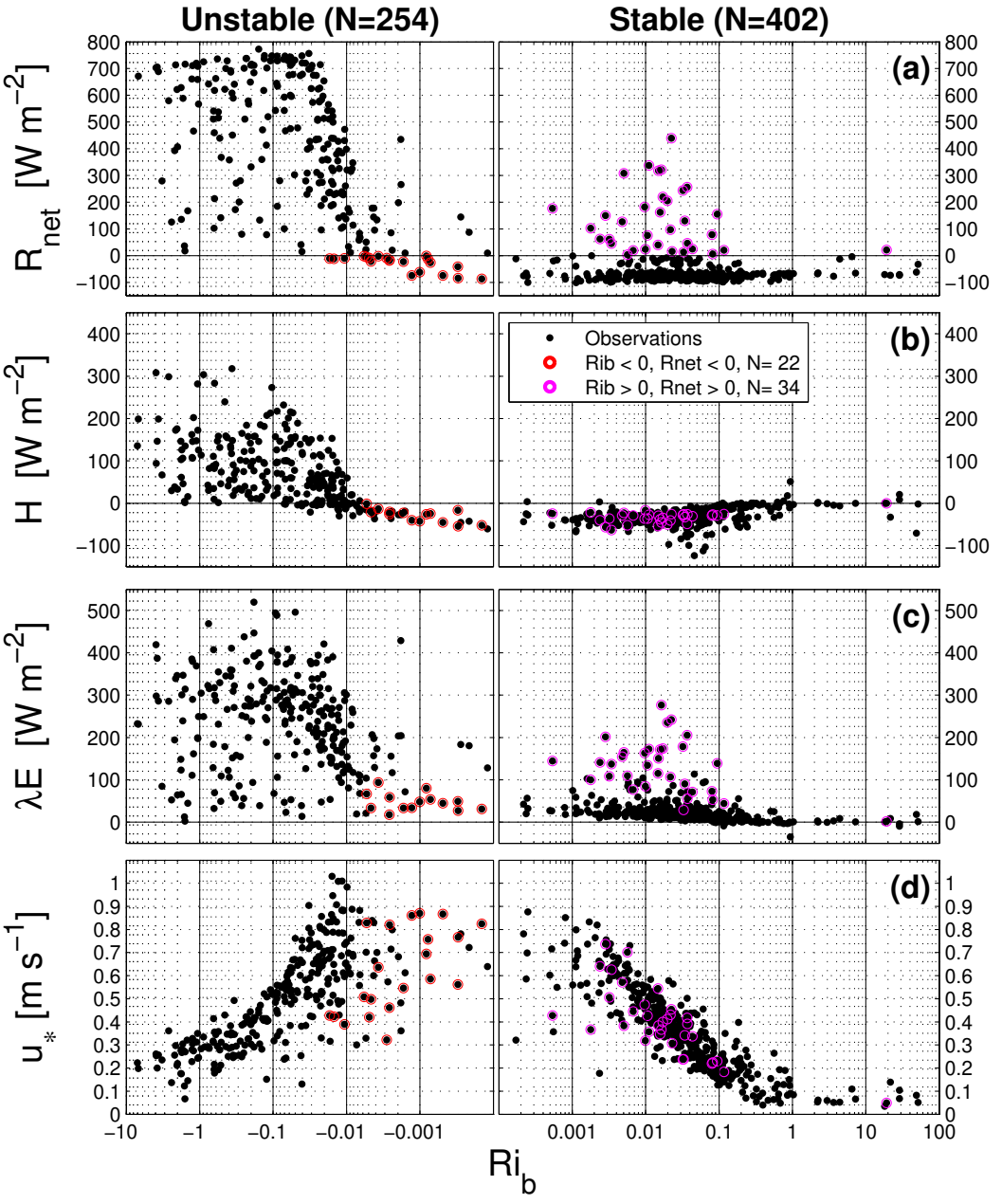

Figure S.5: Scatter plot of the above-canopy 30-min mean values from May 2007 of **(a)** net radiation (R_{net}), **(b)** sensible heat flux (H), **(c)** latent heat flux (λE), and **(d)** friction velocity (u_*) versus the bulk Richardson number (Ri_b). The observation heights are 16 m for R_{net}, 23 m for H and λE, and 10 m for u_*. The number of 30-min samples for the unstable and stable conditions are shown above panel **(a)**. Samples which are considered counter-intuitive are highlighted by the colored circles where the legend contains the number of counter-intuitive samples within each category. The highlighted data points on the stable side (N = 34 points) are excluded from the analyses.

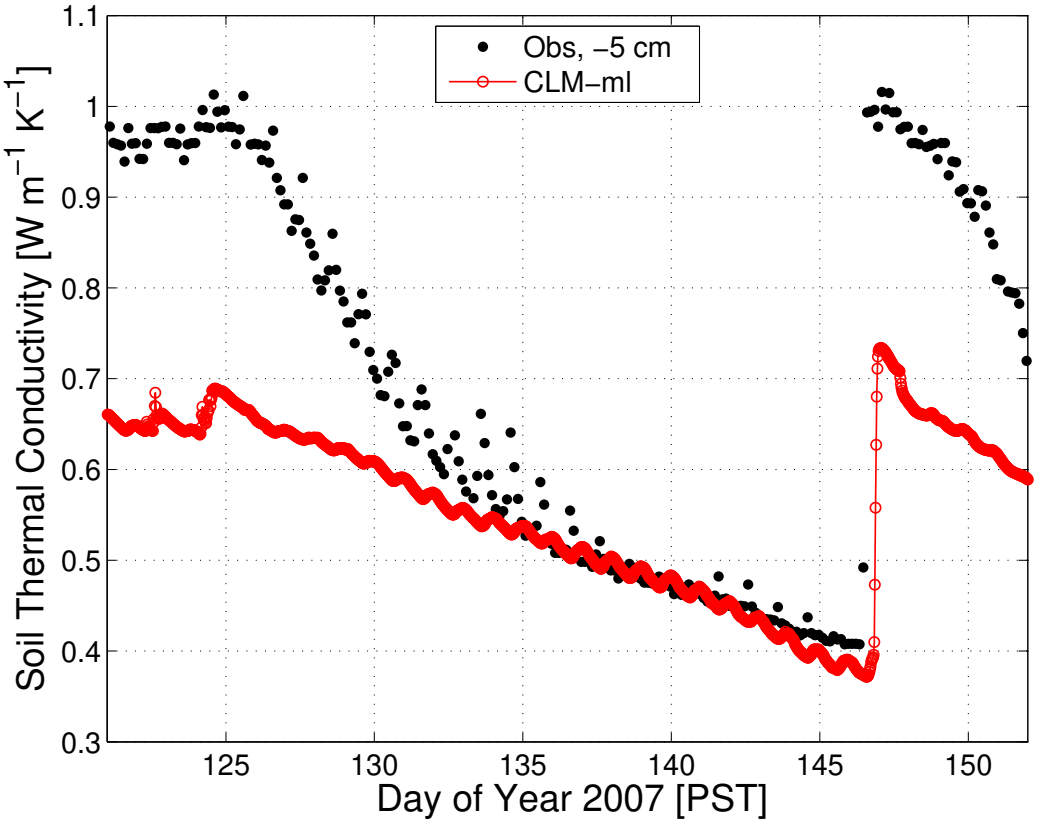

Figure S.6: Time series of observed and modeled soil conductivity. Observed soil conductivity is from a Hukesflux TP01 sensor at a depth of 5 cm.

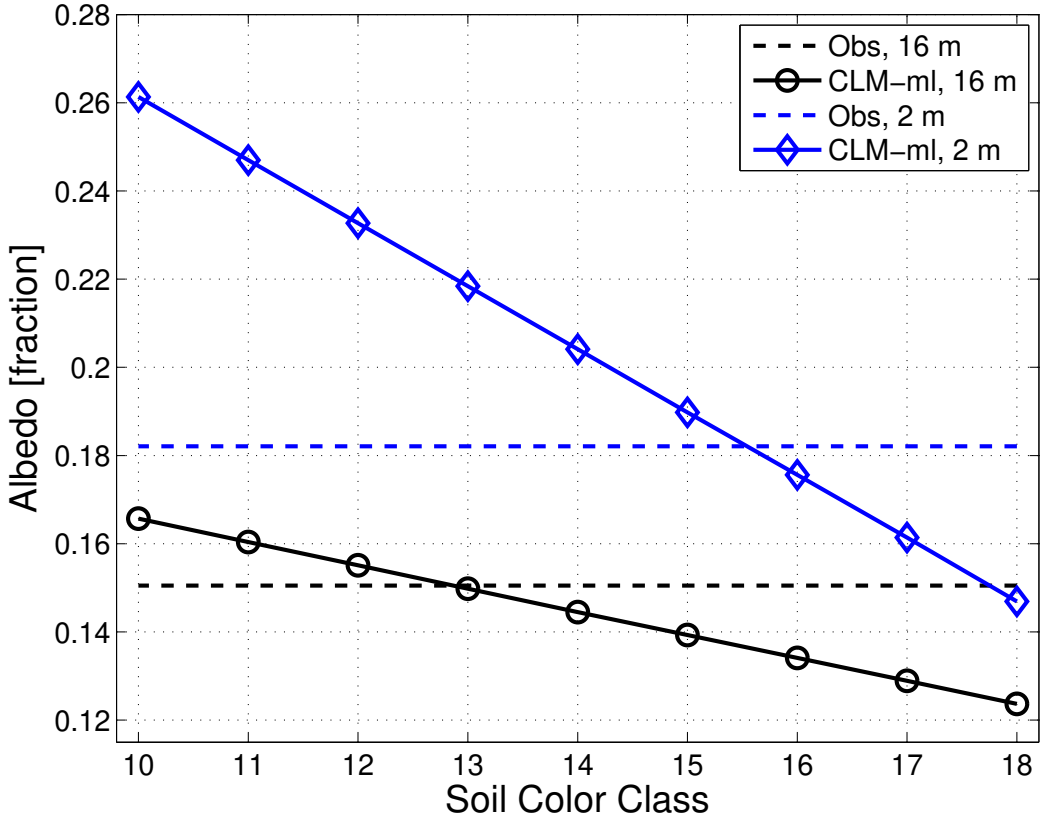

Figure S.7: Observed and modeled 2-m and 16-m albedos in relation to soil color classes 10–18. Albedo is calculated from the average incoming and outgoing shortwave radiation for the period 1–8 April 2007, when observations showed only a small amount of leaves.

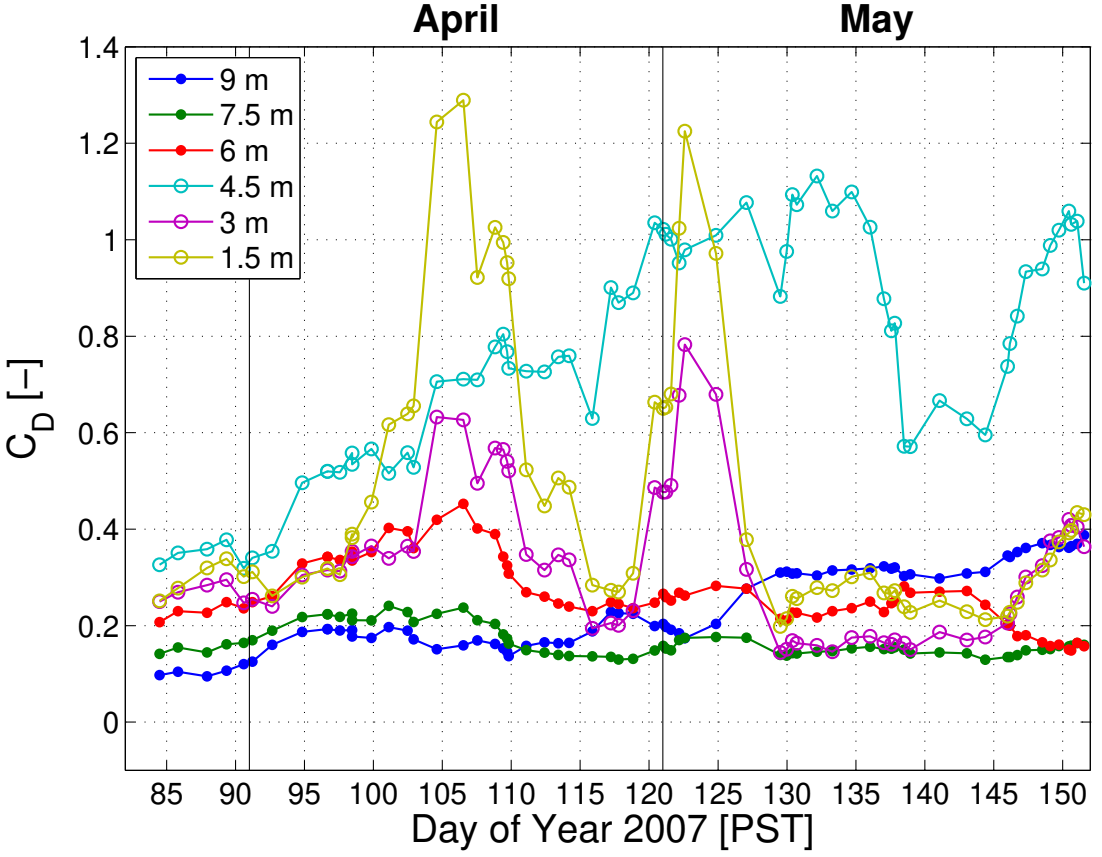

Figure S.8: Time series from late March to the end of May 2007 of the observed local drag coefficient (C_D) at 6 levels within the canopy.

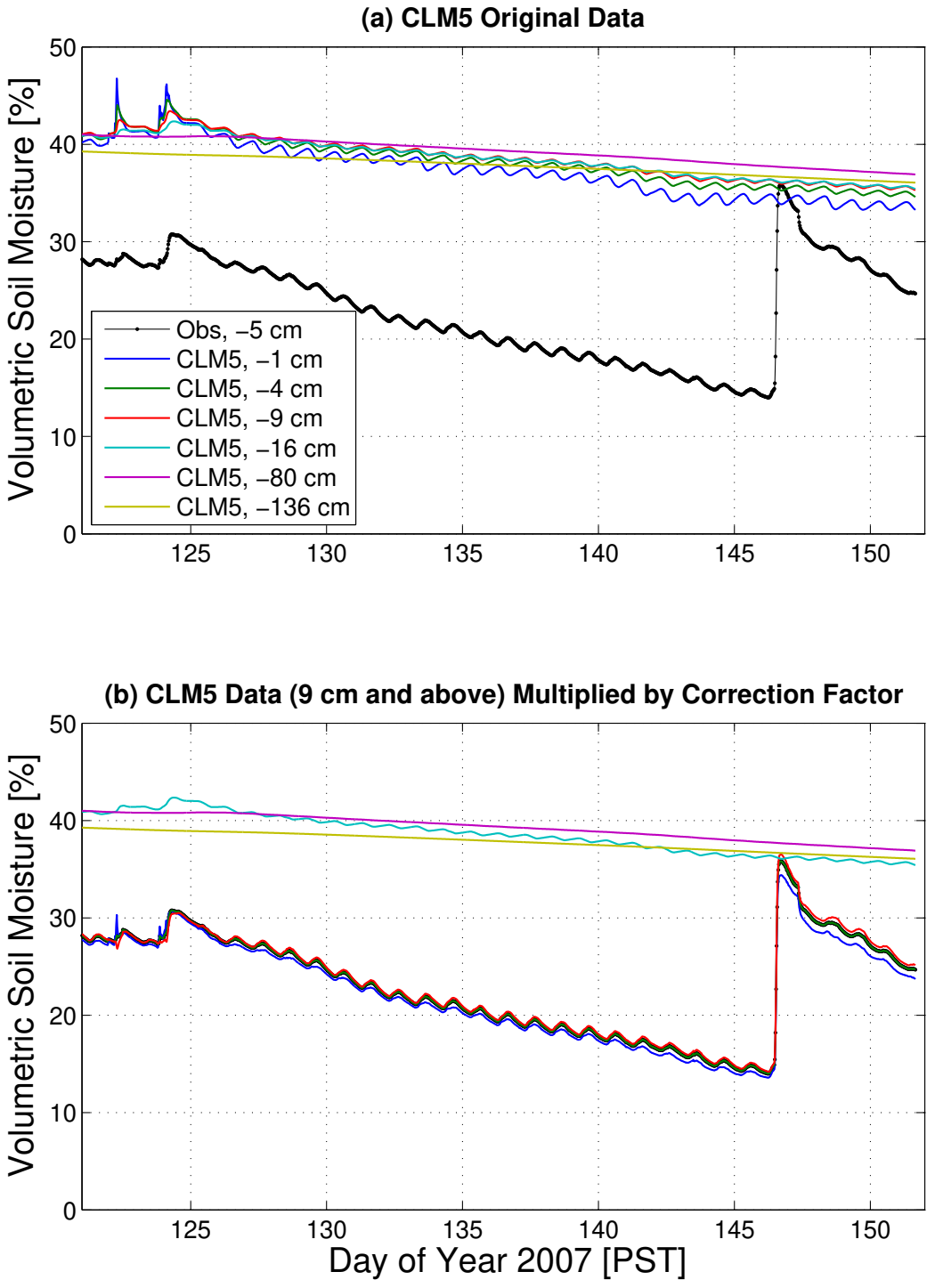

Figure S.9: Time series of **(a)** observed (at 5-cm depth) and CLM5 soil moisture at multiple depths, and **(b)** as in **(a)** but the CLM5 soil moisture above a depth of 9 cm (i.e., the first three soil layers) has been multiplied by a correction factor so that it matches the observed soil moisture.

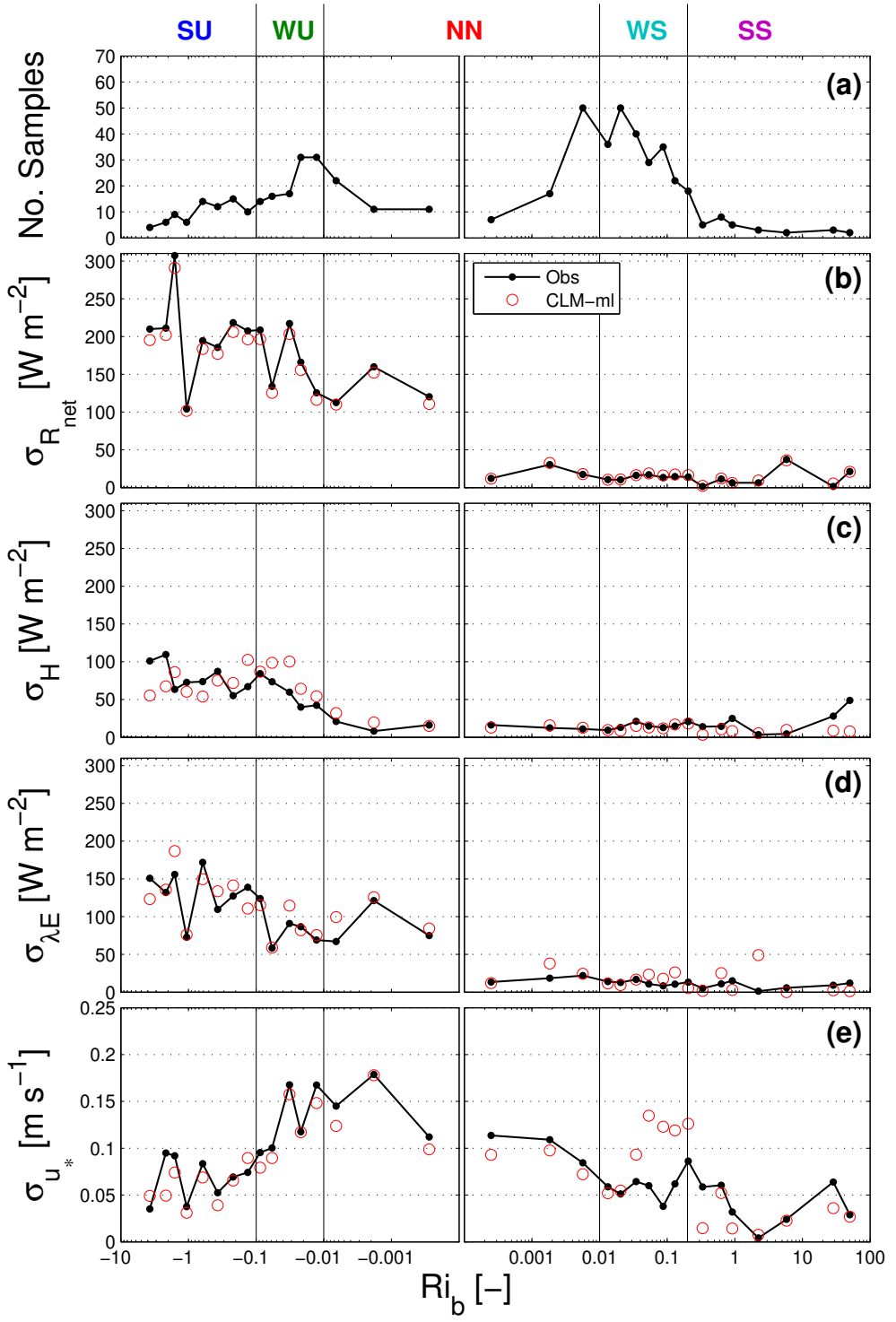

Figure S.10: As in Fig. 10 in the main text, but showing the standard deviation (σ) across the bins for **(b)** net radiation (R_{net}), **(c)** sensible heat flux (H), **(d)** latent heat flux (λE), and **(e)** friction velocity (u_*) for each of the bulk Richardson number (Ri_b) bins.

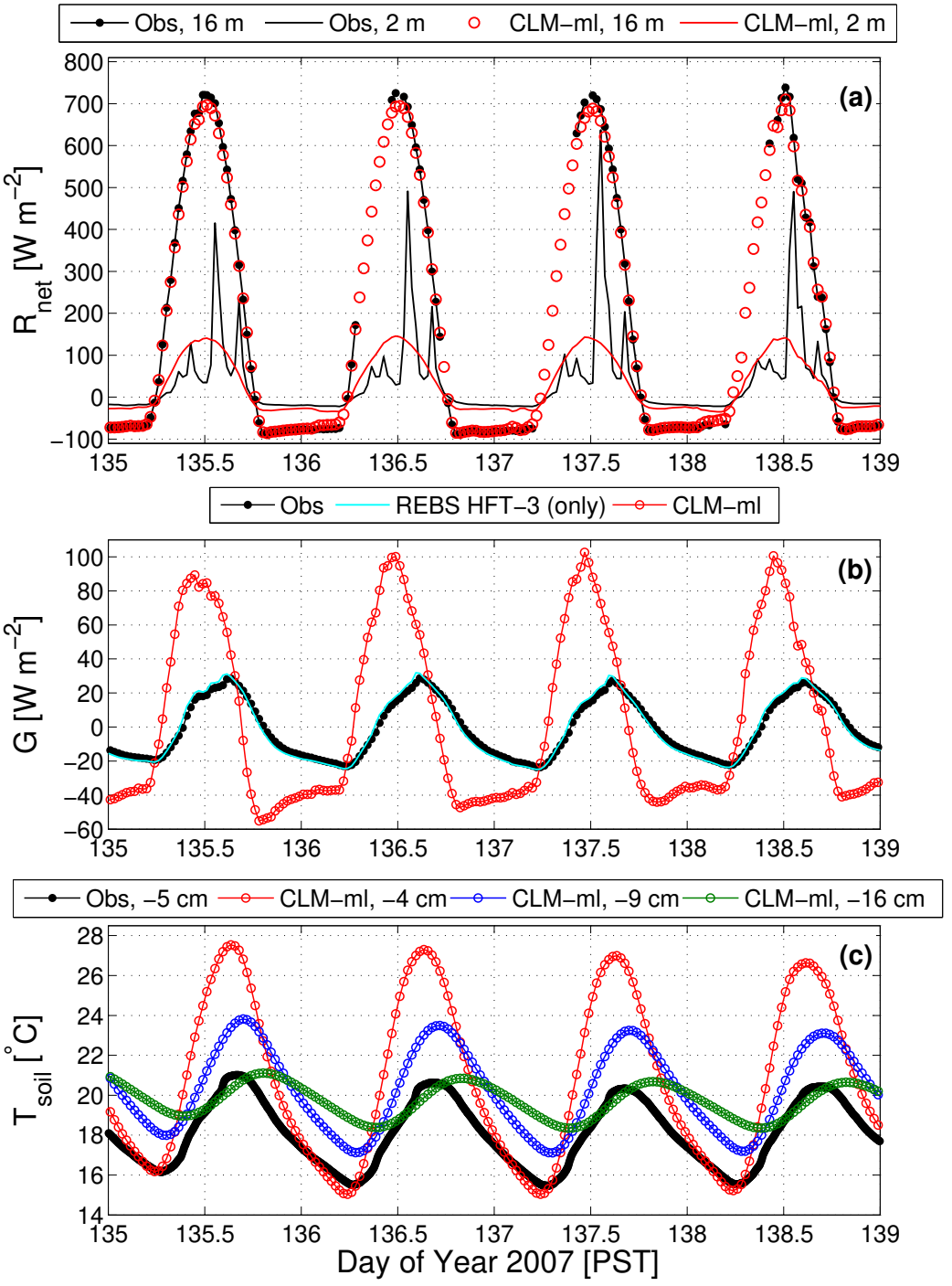

Figure S.11: Time series of observed and CLM-ml **(a)** net radiation (R_{net}) at 16 m and 2 m, **(b)** soil heat flux (G) at the ground surface, and **(c)** soil temperature. For the observations in **(b)**, both the surface soil heat flux (which takes into account the heat stored in the upper soil layers) and the heat flux measured at −5 cm by the REBS HFT-3 soil heat flux plate are shown (see legend).

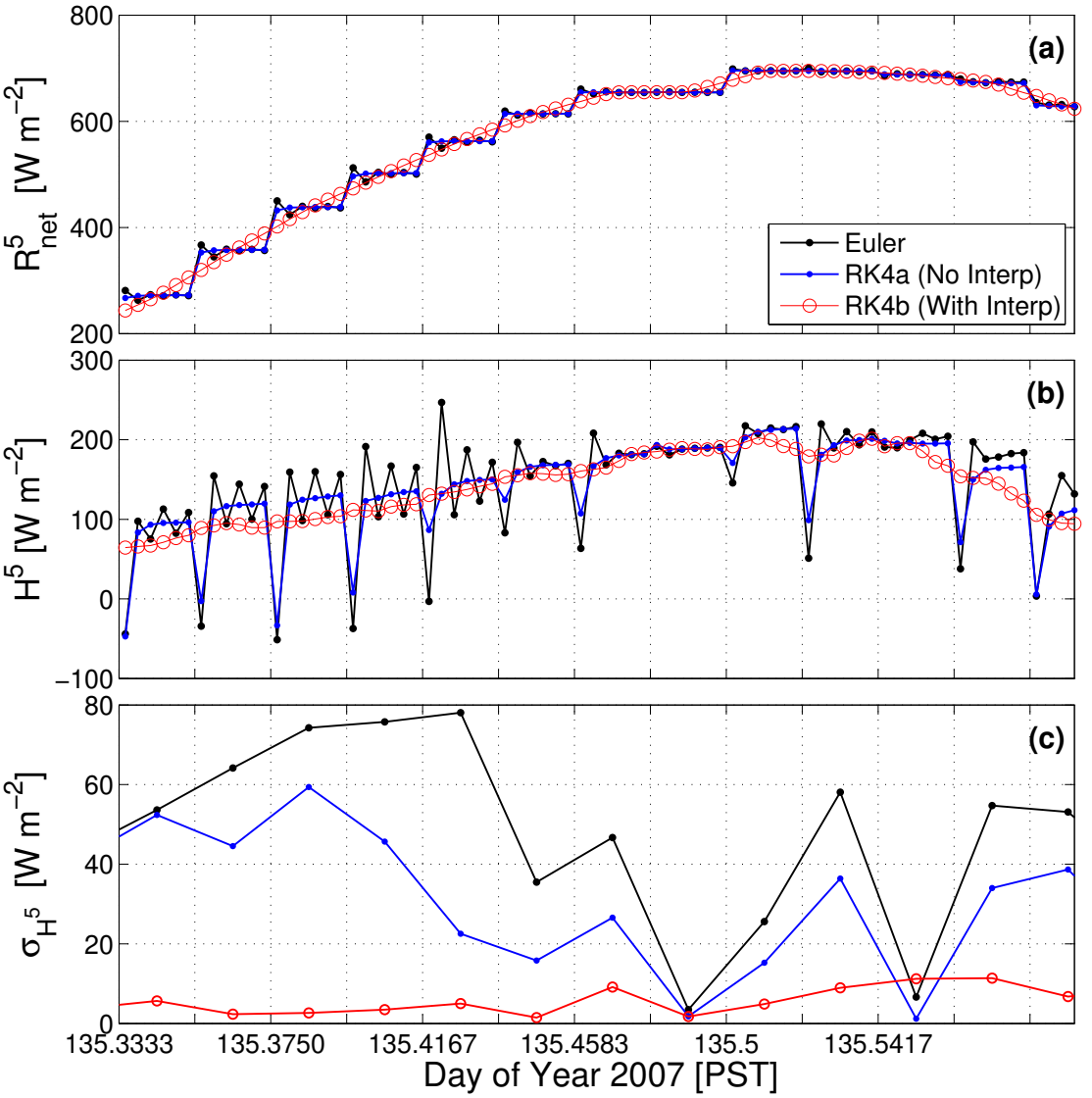

Figure S.12: As in Fig. 15a–c in the main text, but for a different period.

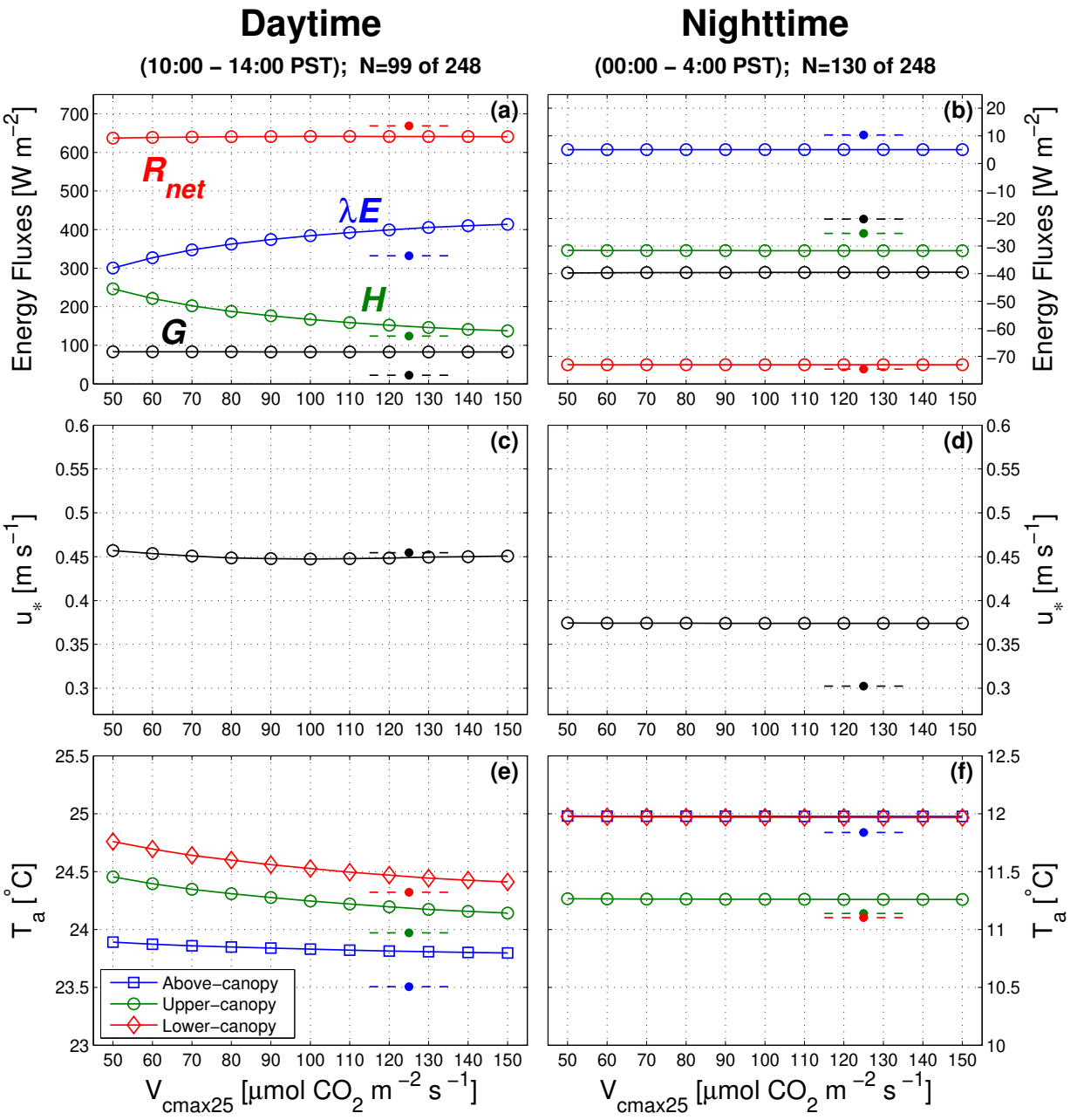

Figure S.13: As in Fig. 16 in the main text, but for variation of the maximum carboxylation rate (V_{cmax25}).

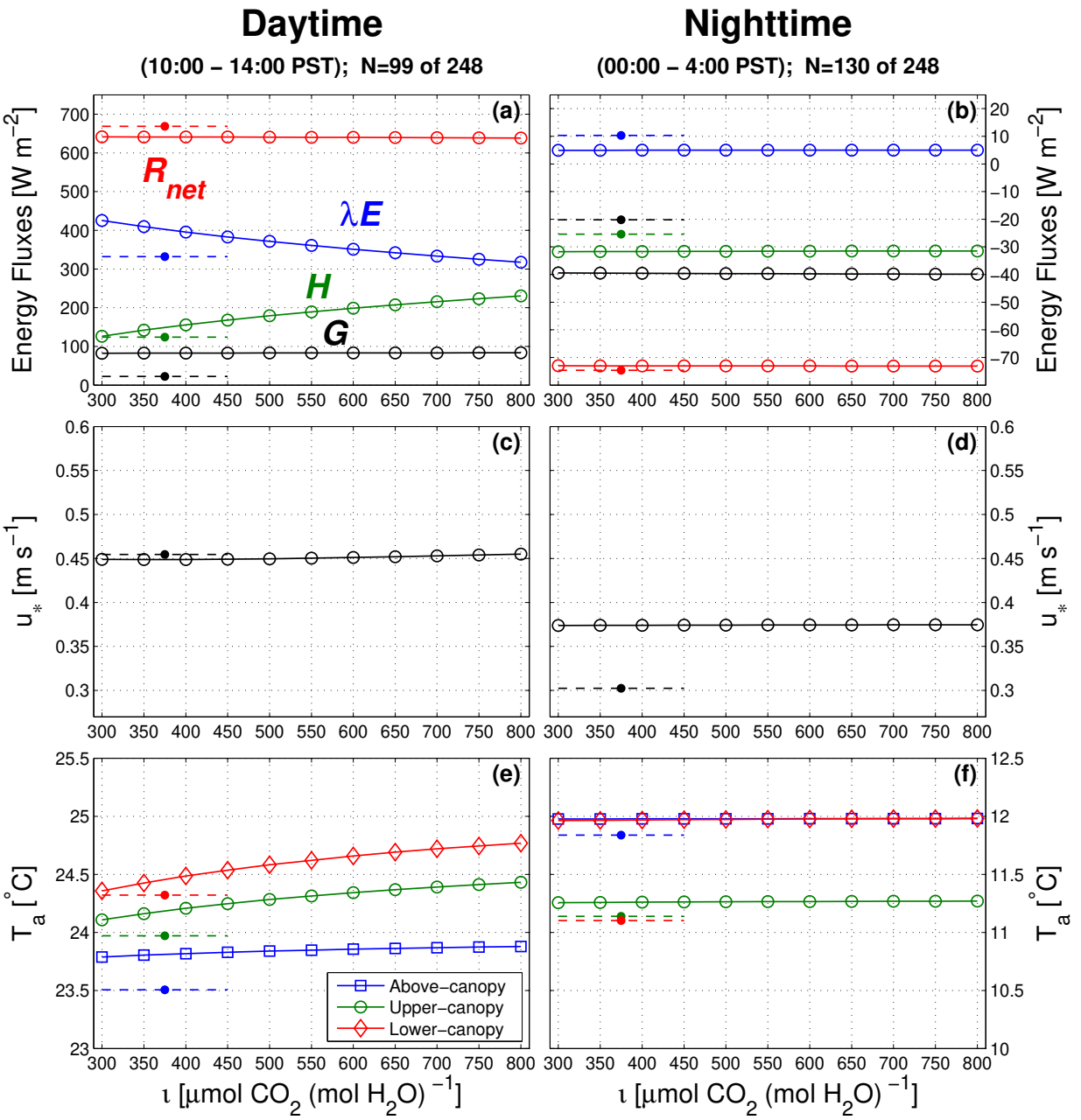

Figure S.14: As in Fig. 16 in the main text, but for variation of the marginal water-use efficiency (ι).

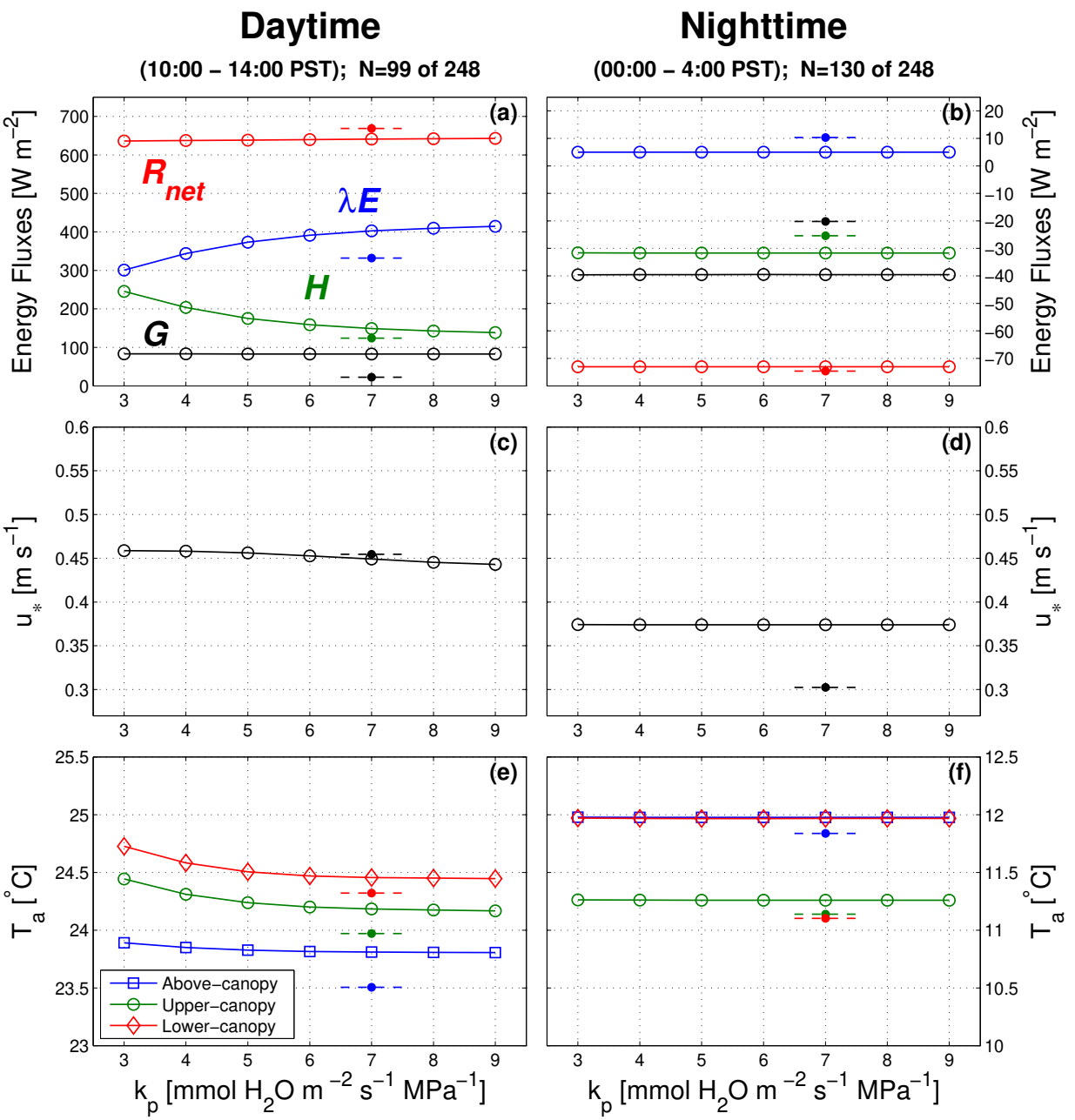

Figure S.15: As in Fig. 16 in the main text, but for variation of the leaf stem conductance (k_p).

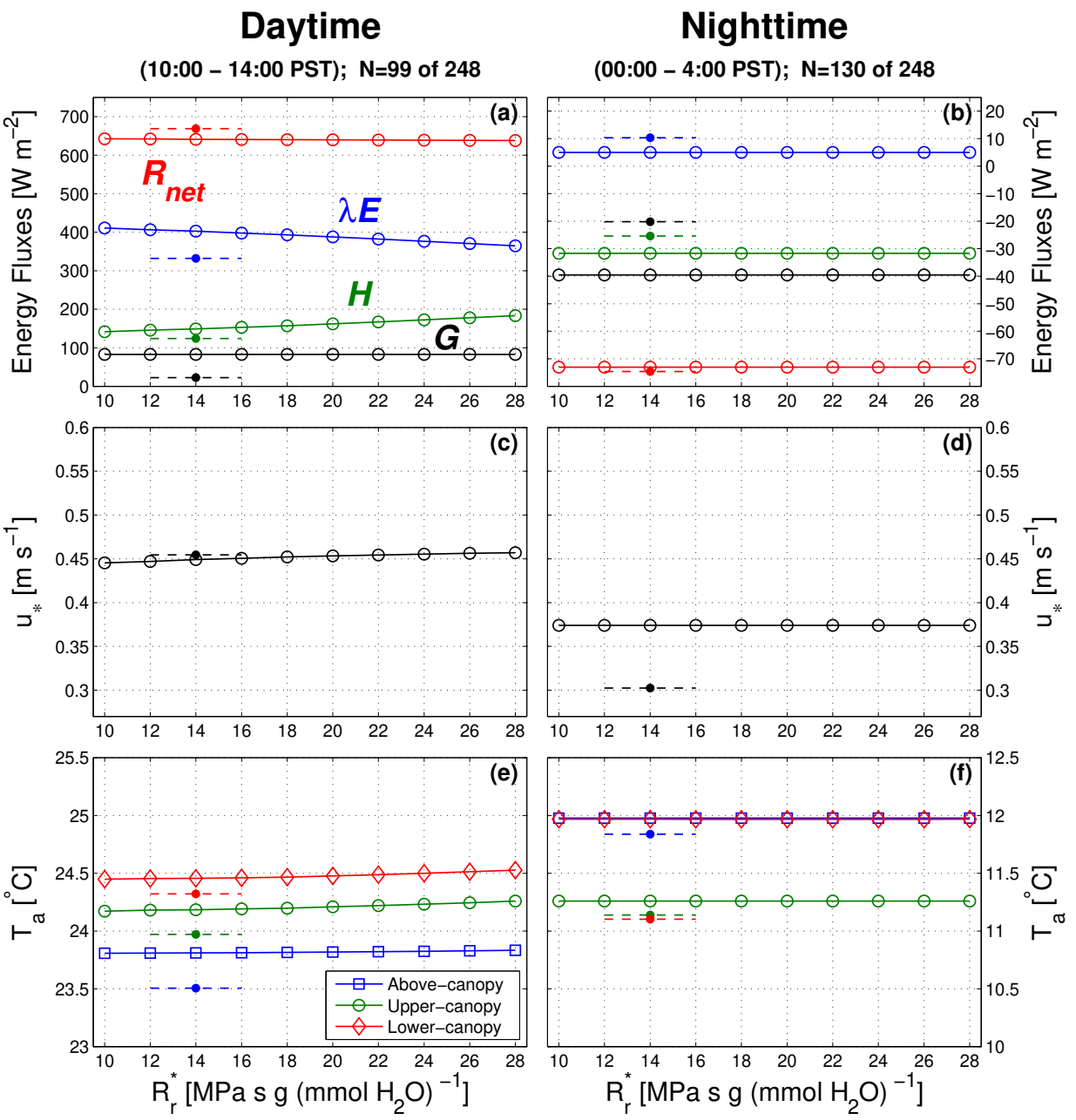

Figure S.16: As in Fig. 16 in the main text, but for variation of the fine root resistivity (R_r^*).

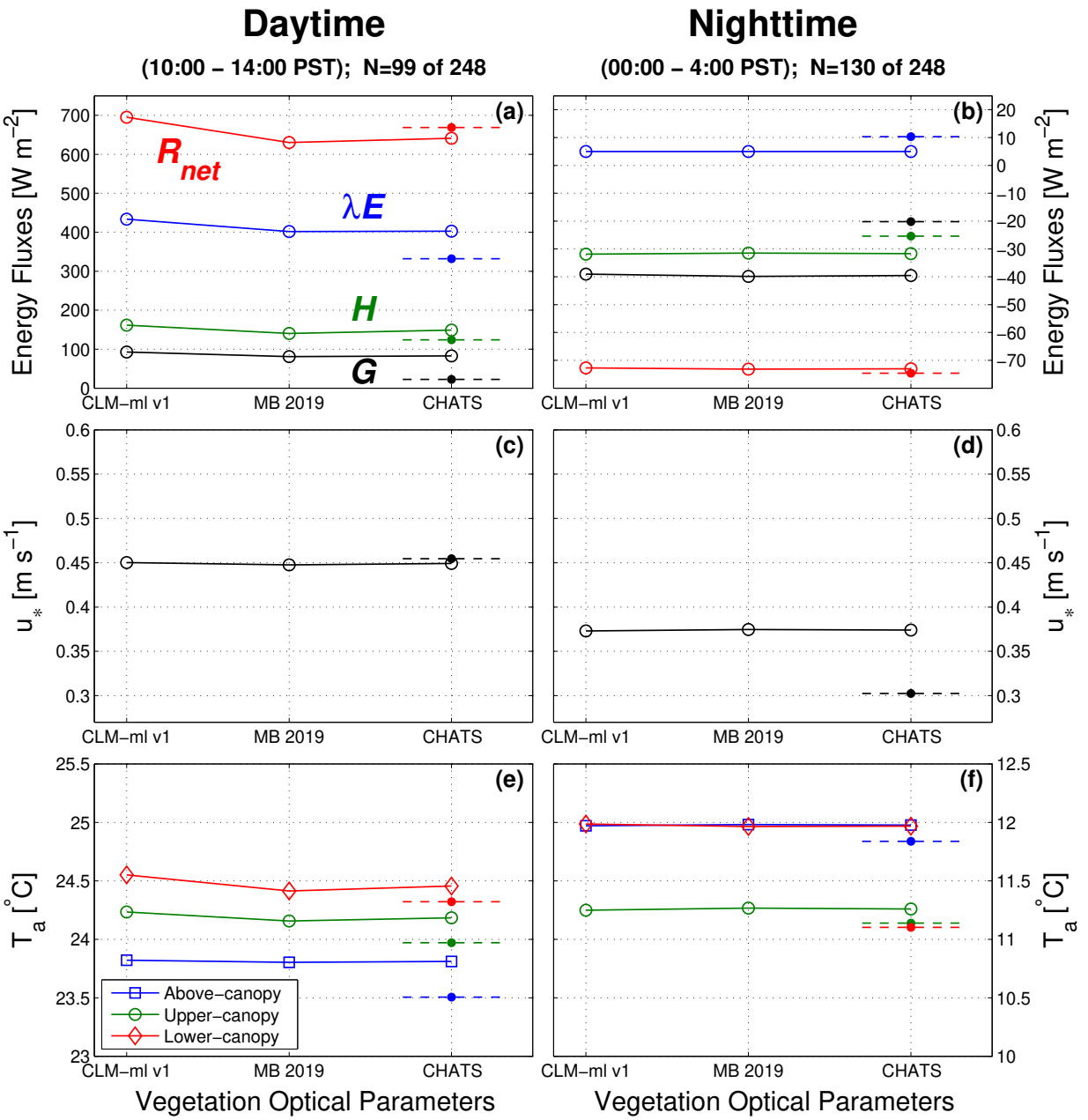

Figure S.17: As in Fig. 16 in the main text, but for variation of the vegetation optical parameters. Parameter values are the CLM-ml v1 default values and the CHATS walnut-specific values given in Table 2 of the main text. Also shown are results using the leaf values proposed by Majasalmi and Bright (2019) for temperate broadleaf deciduous tree: ρ_{leaf}, 0.08 (VIS) and 0.42 (NIR); τ_{leaf}, 0.06 (VIS) and 0.43 (NIR); χ_l, 0.59.

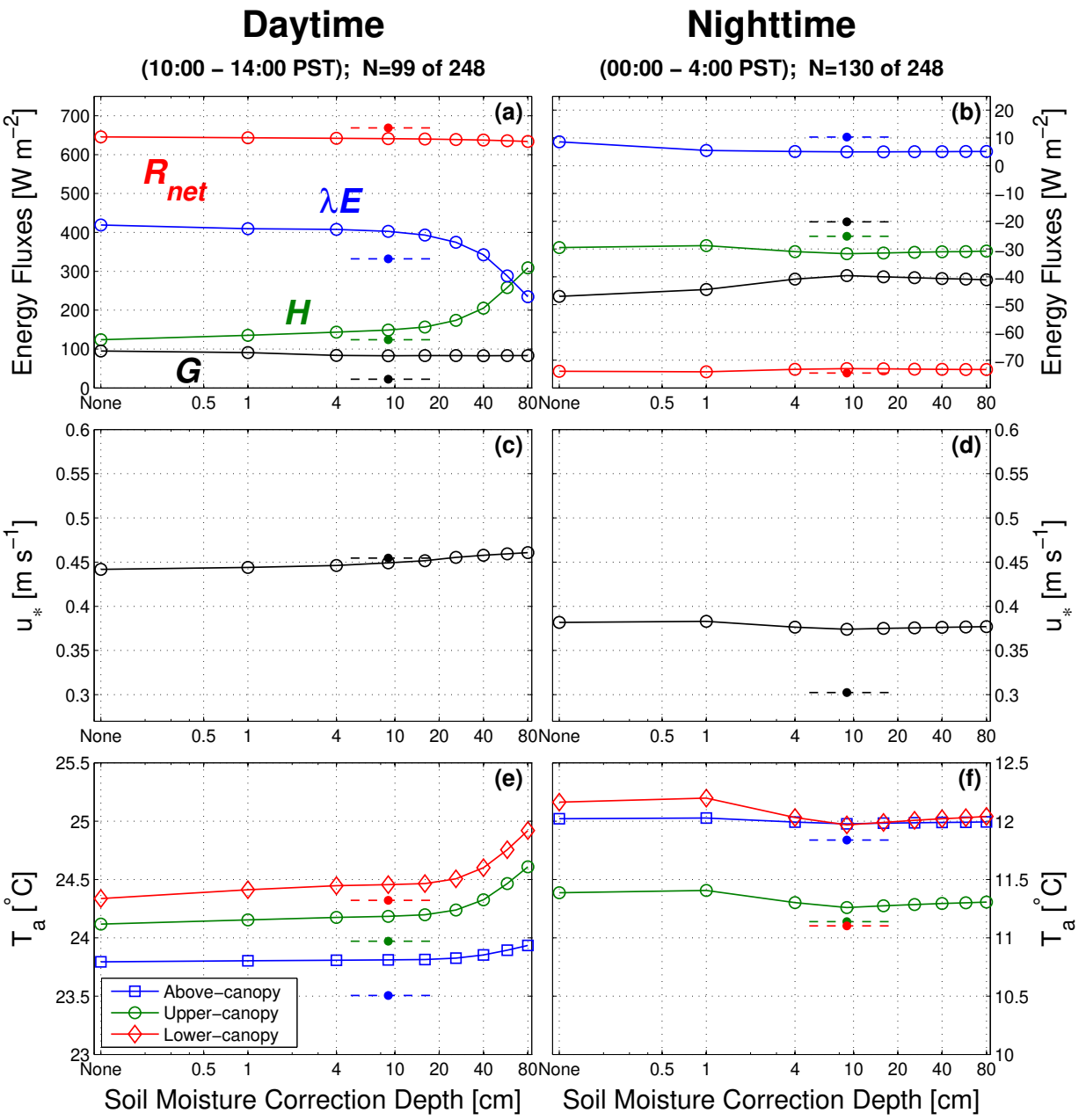

Figure S.18: As in Fig. 16 in the main text, but for variation of the soil moisture correction depth.

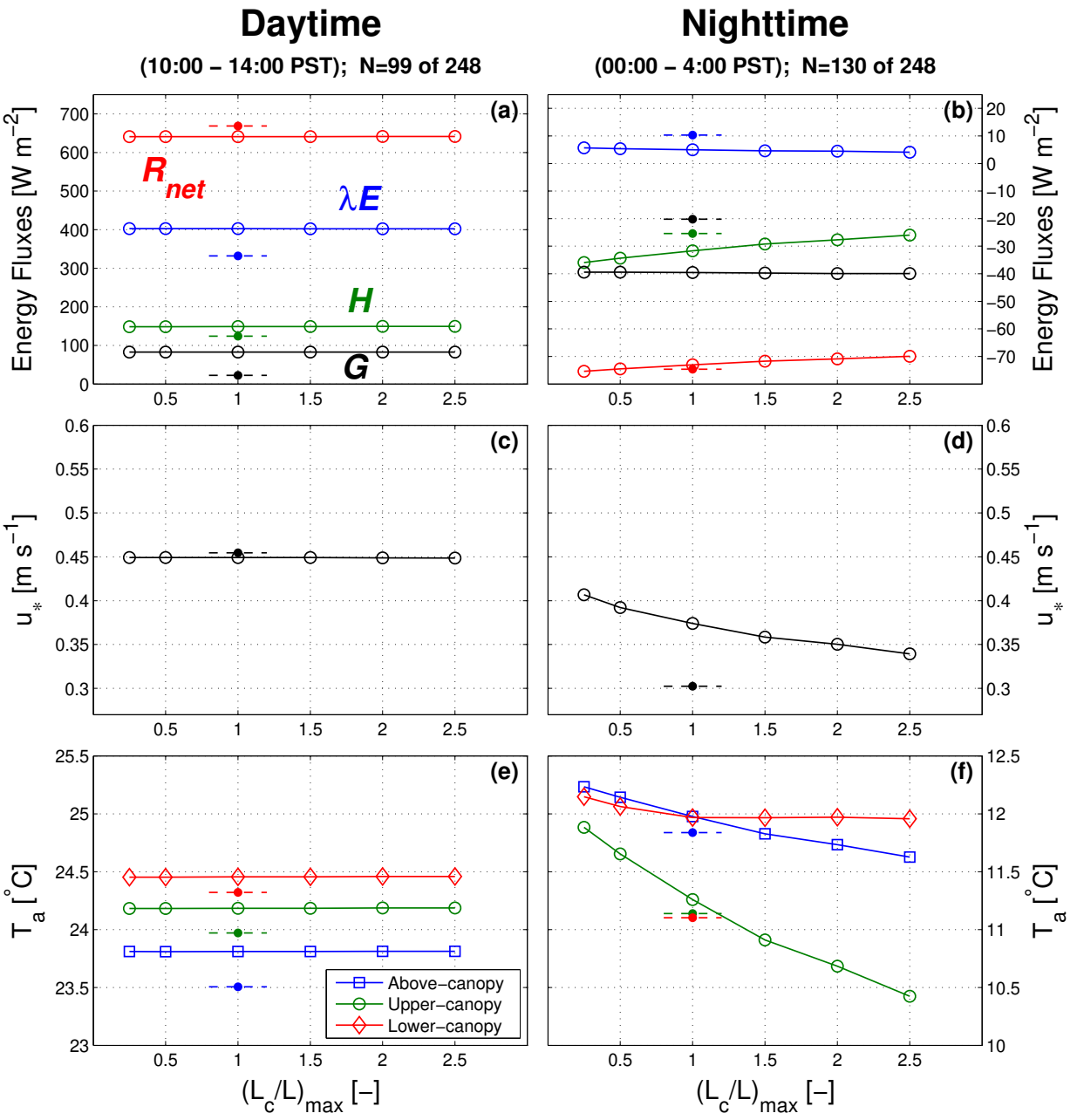

Figure S.19: As in Fig. 16 in the main text, but for variation in the upper limit of L_c/L.

References

Horst, T., 2019. NSF NCAR/EOL ISFS CHATS high rate tower and array data, version 2.0 [dataset]. NSF National Center for Atmospheric Research Earth Observing Laboratory, Boulder, Colorado. doi:10.26023/P4JW-9T0T-QG0S.

Kljun, N., Calanca, P., Rotach, M.W., Schmid, H.P., 2015. A simple two-dimensional parameterisation for Flux Footprint Prediction (FFP). Geosci. Model Dev. 8, 3695–3713. doi:10.5194/gmd-8-3695-2015.

Majasalmi, T., Bright, R.M., 2019. Evaluation of leaf-level optical properties employed in land surface models. Geosci. Model Dev. 12, 3923–3938. doi:10.5194/gmd-12-3923-2019.